LETTER

doi:10.1038/nature10104

Improved measurement of the shape of the electron

J. J. Hudson[1], D. M. Kara[1], I. J. Smallman[1], B. E. Sauer[1], M. R. Tarbutt[1] & E. A. Hinds[1]

The electron is predicted to be slightly aspheric[1], with a distortion characterized by the electric dipole moment (EDM), d_e. No experiment has ever detected this deviation. The standard model of particle physics predicts that d_e is far too small to detect[2], being some eleven orders of magnitude smaller than the current experimental sensitivity. However, many extensions to the standard model naturally predict much larger values of d_e that should be detectable[3]. This makes the search for the electron EDM a powerful way to search for new physics and constrain the possible extensions. In particular, the popular idea that new supersymmetric particles may exist at masses of a few hundred GeV/c^2 (where c is the speed of light) is difficult to reconcile with the absence of an electron EDM at the present limit of sensitivity[2,4]. The size of the EDM is also intimately related to the question of why the Universe has so little antimatter. If the reason is that some undiscovered particle interaction[5] breaks the symmetry between matter and antimatter, this should result in a measurable EDM in most models of particle physics[2]. Here we use cold polar molecules to measure the electron EDM at the highest level of precision reported so far, providing a constraint on any possible new interactions. We obtain $d_e = (-2.4 \pm 5.7_{stat} \pm 1.5_{syst}) \times 10^{-28} e$ cm, where e is the charge on the electron, which sets a new upper limit of $|d_e| < 10.5 \times 10^{-28} e$ cm with 90 per cent confidence. This result, consistent with zero, indicates that the electron is spherical at this improved level of precision. Our measurement of atto-electronvolt energy shifts in a molecule probes new physics at the tera-electronvolt energy scale[2].

Just as a magnetic dipole moment $\boldsymbol{\mu}$ in a magnetic field $\mathbf{B}$ has an energy $-\boldsymbol{\mu} \cdot \mathbf{B}$, an electric dipole moment $\mathbf{d}$ in an electric field $\mathbf{E}$ has an energy $-\mathbf{d} \cdot \mathbf{E}$ in the non-relativistic limit. A permanent EDM of the electron must lie along its spin[6], $\boldsymbol{\sigma}$, that is, $\mathbf{d} = d_e\boldsymbol{\sigma}$, making the electron's energy depend on whether the spin is parallel or antiparallel to $\mathbf{E}$. In an atom or molecule with an unpaired valence electron, the interaction of the electron EDM with an applied electric field results in an energy difference between two states that differ only in their spin orientation. This energy difference is proportional to d_e and changes sign when the direction of the field is reversed. A sensitive method of measuring this energy difference is to align the spin perpendicular to the field and measure its precession rate, which is proportional to the energy difference. An alternative description of the method is in terms of an interferometer. There is quantum interference between the two spin states, and the EDM appears as an interferometer phase shift that changes sign when the electric field is reversed.

To improve on the previous limit[7] we developed a technique using the dipolar molecule YbF (ref. 8) instead of the spherical Tl atom. This has two great advantages. First, at our modest operating field the interaction energy[9–15] of YbF due to d_e is 220 times larger than that obtained using Tl in a much larger field[7]. Second, the motional magnetic field, a source of systematic error that plagued the Tl experiment, has a negligible effect on YbF (ref. 8). Because of these advantages, it is possible to improve on the Tl experiment by using YbF molecules, even though the molecules are produced in much smaller numbers. A number of other EDM measurements, based on electron spin precession in atoms, molecules, molecular ions or solids, are in progress[4].

Figure 1 shows the interferometer apparatus[16]. Pulses of YbF molecules are emitted by the source[17]. The experiment uses those molecules in the $F = 0$ and $F = 1$ hyperfine levels of the ground state. The molecules pass through a first fluorescence detector, the pump detector, which simultaneously measures and empties out the $F = 1$ population. Then they enter a pair of electric field plates, between which are static electric and magnetic fields $(E, B)\hat{\mathbf{z}}$, where $\hat{\mathbf{z}}$ is the unit vector in the z direction (Fig. 1). This region is magnetically shielded. A radio-frequency (r.f.) pulse is applied to transfer molecules from $|F, m_F\rangle = |0, 0\rangle$ to the state $\frac{1}{\sqrt{2}}(|1, +1\rangle + |1, -1\rangle)$, where m_F is the component of the total angular momentum, F, along the z-axis. The molecules then evolve freely for a time T, during which the $m_F = \pm 1$ components develop a phase difference of $2\phi = 2(\mu_B B - d_e E_{eff})T/\hbar$, where μ_B is the Bohr magneton. This is due to the Zeeman shift $+\mu_B B m_F$ (ref. 18) and to the EDM shift expressed by the effective interaction $-d_e E_{eff} m_F$ (see Methods). A second r.f. pulse is then applied, resulting in a final $F = 0$ population proportional to $\cos^2\phi$, which the second fluorescence detector subsequently measures. For every pulse of molecules, the time-resolved signals from the pump and probe detectors are recorded; an example probe signal is shown in Fig. 2.

Scanning the phase difference via the magnetic field generates an interference curve, shown in Fig. 3. Reversal of the applied electric field produces a small phase shift $\delta\phi = 2d_e E_{eff} T/\hbar$, leading to a change in the detector count of $\delta I = (\mathrm{d}I/\mathrm{d}\phi)\delta\phi$. This is maximized by operating the interferometer at $B = \pm 13.6$ nT, which corresponds to $\phi = \pm\pi/4$, the steepest points on either side of the central fringe (Fig. 3). The intensity change is opposite on the two sides of the fringe because the slopes are opposite. Thus the EDM signal δI is the part of the fluorescence count that is correlated with the sign of $E \cdot B$. We calibrate the slope $\mathrm{d}I/\mathrm{d}\phi$ by making a step $\delta B = \pm 1.7$ nT in magnetic-field magnitude, and this too is done on each side of the central fringe. In addition to E, B and δB, several other parameters are switched in the experiment. The laser frequency is stepped by ± 340 kHz, the frequencies of the two r.f. pulses (ν_{rf1} and ν_{rf2}) are independently stepped by ± 1.5 kHz, their amplitudes (a_{rf1} and a_{rf2}) are independently stepped by $\pm 5\%$, and the phase difference (Φ_{rf}) between them is stepped around a randomly chosen value, ϕ_0, by $\pm\pi/2$. A computer places the machine in a new switch state before every beam pulse. The measurements are grouped into 'blocks' of 4,096 beam pulses, over which all 512 combinations of switch states are covered equally. Error signals, derived from each

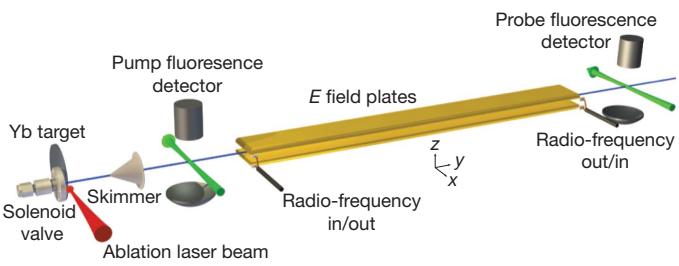

Figure 1 | Schematic diagram of the pulsed molecular beam apparatus.

[1]Centre for Cold Matter, Blackett Laboratory, Imperial College London, Prince Consort Road, London SW7 2AZ, UK.

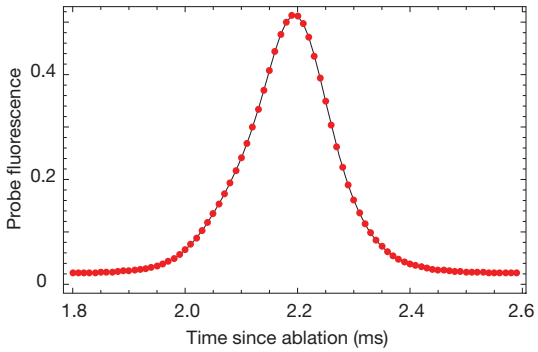

Figure 2 | Fluorescence from a typical beam pulse, measured on the probe detector.

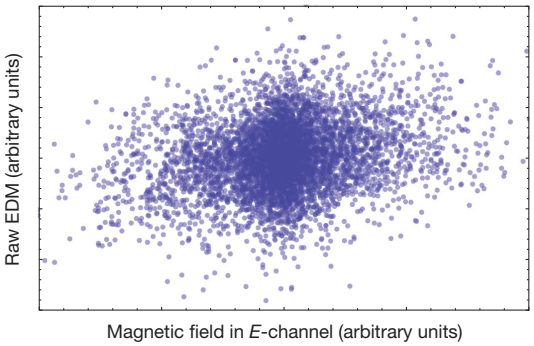

Figure 4 | The magnetic field correlated with the E reversal, measured at the fluxgate magnetometer, versus the EDM values. A slope is evident. The majority of measurements are not significantly perturbed by the magnetic field, but a small fraction do benefit from correction.

block of data, are fed back to the switched parameters to keep them switching around their optima.

Our measurement is derived from 6,194 blocks of data taken in 2010, comprising 25 million molecular beam pulses, together with many subsidiary measurements used to search for systematic errors. To analyse the data, we select the central 130 μs of each probe pulse (Fig. 2) and normalize it pulse by pulse to the pump fluorescence. This minimizes the effect of fluctuations of the molecular beam intensity. We calculate how much of the gated, normalized fluorescence signal is correlated with all 512 possible combinations of the modulated parameters. These correlations are called 'channels' and are denoted by $\{X\}$, where X indicates the parameter (or parameter combination) being modulated. The EDM phase shift, normalized to the shift from the small magnetic field step δB, is $\{E \cdot B\}/\{\delta B\}$. The other channels are valuable in elucidating the operation of the apparatus. Throughout the investigation the EDM values were concealed by adding a fixed unknown offset, which was only removed once the data collection and analysis were complete.

The EDM values obtained from the set of blocks are almost normally distributed but there tend to be a few more points in the wings of the distribution than in a normal distribution. The same is true of other quantities of interest that we extract from the data. For all these quantities, we calculate the 5% trimmed mean[19], a simple robust statistic that drops the largest and smallest 5% of the data. We use the bootstrap method[20] to determine the associated statistical uncertainty. For non-normal distributions, these methods give more reliable measures than the mean and standard error.

Fluctuations in the ambient magnetic field of the laboratory inevitably have some component that is, by chance, synchronous with the switching pattern of E. This contributes a little to the noise in the EDM, as shown in Fig. 4, though not to the long-time average value. We suppress this excess noise by correcting the EDM, block by block, according to the magnetic field readings of a magnetometer (Methods). The central value and statistical uncertainty of this magnetic field correction are given in Table 1. The correction has a negligible effect on the central value of the EDM but reduces the statistical error by 3.5%.

We find that the phase of the interferometer shifts linearly with the detunings of the r.f. pulses at a rate of $(283 \pm 6) \times 10^{-9}$ rad Hz^{-1} for the first r.f. pulse, and $(-94 \pm 5) \times 10^{-9}$ rad Hz^{-1} for the second r.f. pulse. If the magnitude of the electric field changes when E is reversed, then through the Stark shift, the r.f. transition frequency changes. This results in a change in the interferometer phase that correlates with E, mimicking the EDM phase. This systematic error can be corrected using the information contained in every block of data. The phase change resulting from a detuning of the first r.f. pulse is measured by $\{v_{rf1} \cdot B\}$, and the change in the detuning resulting from the change in electric field magnitude is measured by $\{v_{rf1} \cdot E\}$. The product of these two channels, together with a calibration factor that we have measured, determines the EDM-like phase due to the E-correlated detuning of the first r.f. transition, and we use this to apply a correction to each block of data. A similar correction is made for the second r.f. pulse. The central values and statistical uncertainties of the two r.f. phase corrections are given in Table 1. As an additional check, we made measurements in which we deliberately change the r.f. frequency when we switch E. We see that the resulting systematic error is entirely removed once the corrections are applied to these data, thus verifying the correction procedure.

There are several sources of systematic uncertainty on the EDM measurement that must be considered. First, there may be systematic effects, other than the r.f.-induced phases described above, caused by a change in field magnitude when E reverses. We investigate this by changing the field magnitude intentionally by δE when the field switches. Once the r.f. phase corrections are applied to these data,

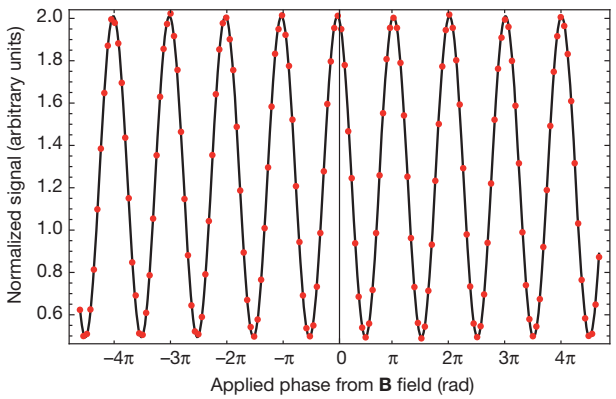

Figure 3 | Interferometer fringes produced by magnetic field scan. Dots indicate the probe fluorescence normalized to the pump fluorescence. The line is the fit to the cosine-squared model.

Table 1 | Summary of applied corrections and uncorrected systematic uncertainties

	Correction	Statistical	Systematic
Magnetic-field correction	−0.3	1.7	<0.1
rf1 phase correction	5.0	0.9	<0.1
rf2 phase correction	0.5	0.7	<0.01
Uncorrected δE effects	–	–	1.1
$\bar{V}$ uncertainty	–	–	0.1
$\{v_{rf1}\}$ correlation	–	–	1.0
Geometric phase	–	–	0.03
Leakage currents	–	–	0.2
Shield magnetization	–	–	0.25
$\mathbf{v} \times \mathbf{E}$ effect	–	–	0.0005

The units are $10^{-28} e$ cm. The statistical uncertainty on the corrections gives a measure of their random spread over the whole data set. In the final analysis the corrections are applied block-by-block, so these statistical uncertainties are naturally incorporated in the final EDM statistical uncertainty. The systematic uncertainty in the corrections is negligible.

we find no evidence of any residual systematic EDM that depends on δE. The upper bound on the gradient of any such systematic, with respect to δE, is $-11 \times 10^{-28} e\,\mathrm{cm/(V\,cm^{-1})}$. In the r.f. regions we measure asymmetries δE of approximately 100 mV cm^{-1} and we take this to be typical throughout the interaction region. Combining this level of asymmetry with the worst-case slope above gives a systematic uncertainty of $1.1 \times 10^{-28} e$ cm (Table 1).

Electric-field-plate potentials that are not symmetric around the ground potential are another possible source of systematic error. We characterize this in terms of the mean potential $\bar{V}$ of the two electric field plates relative to the surrounding grounded apparatus. Near the edges of the plates, the field does not point entirely along $\hat{\mathbf{z}}$, but the direction of the field reverses perfectly as long as $\bar{V} = 0$. However, when $\bar{V} \neq 0$ the reversal is imperfect, and this, coupled with other imperfections, may result in a systematic error. We investigate this by deliberately applying large mean potentials of $\bar{V} = -1{,}000.5$ V and $\bar{V} = +1{,}015.0$ V, and we find from this data a systematic shift with a slope of $(0.099 \pm 0.016) \times 10^{-28} e\,\mathrm{cm\,V^{-1}}$. The plate potentials used for our data set are measured to have a mean voltage of less than 1 V. This results in a systematic uncertainty of $0.1 \times 10^{-28} e$ cm.

A study of the data taken at non-zero $\bar{V}$ revealed an unexplained correlation between the measured EDM and the frequency detuning of the first r.f. pulse. Unlike the effect described above, this systematic effect does not depend on δE. We see no evidence of the effect in the data taken at $\bar{V} = 0$. Nonetheless, by considering the worst-case correlation consistent with the $\bar{V} = 0$ data, and the measured average frequency detuning of the first r.f. pulse, we calculate a conservative systematic uncertainty of $1 \times 10^{-28} e$ cm.

The direction of the electric field in the rest frame of the molecules rotates slightly as they move through the apparatus. This induces a geometric interferometer phase that can result in a systematic error[21]. We calculate an upper limit on this effect (see Supplementary Information) of $3 \times 10^{-30} e$ cm.

Magnetic fields generated inside the magnetic shields that reverse with the electric field are a potential source of systematic error. These magnetic fields are not well sensed by the magnetometers, which are outside the inner layer of magnetic shielding. We consider the three mechanisms that could generate such fields:

(1) Leakage current to the high-voltage plates. The current flowing to or from each electric field plate is monitored[22] throughout the experiment. The component that reverses synchronously with E is less than 1 nA averaged over the EDM data set. A most conservative estimate (see Supplementary Information) of the possible false EDM given by these currents is $0.2 \times 10^{-28} e$ cm.

(2) Inner-shield magnetization. It is possible that the plate-charging currents could magnetize the shields, generating a magnetic field that reverses with E. We have determined this field by pulsing a hundred times the normal current through a similar shield set-up on the bench and measuring the resulting field with a fluxgate magnetometer. We deduce that the false EDM due to shield magnetization is $(-0.16 \pm 0.17) \times 10^{-28} e$ cm. As this is consistent with zero, we do not make any correction to the measured EDM, but allow a systematic uncertainty of $0.25 \times 10^{-28} e$ cm.

(3) Motional magnetic field. The laboratory-frame electric field has a magnetic component in the rest frame of the molecules $\mathbf{B}_\mathrm{m} = \mathbf{E} \times \mathbf{v}/c^2$, where $\mathbf{v}$ is the velocity of the molecules with respect to the apparatus. This can produce a false EDM if there is also a stray magnetic field B_y. This was a limiting systematic error in ref. 7. The effect is strongly suppressed in our case because of the large (8 MHz) tensor Stark splitting of the $F = 1$ manifold, which renders the molecule insensitive to magnetic fields in the x–y plane, as discussed in ref. 8. Our stray B_y is everywhere less than 30 nT, which gives a calculated false EDM of less than $5 \times 10^{-32} e$ cm. We have also checked empirically that the addition of a 500 nT transverse field produces no evident effect.

A number of other consistency checks and searches for systematic errors were made and are described in detail in the Supplementary Information.

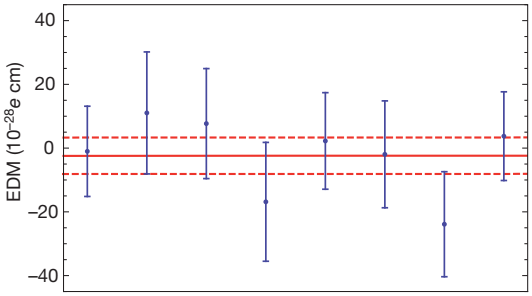

Figure 5 | EDM values for each manual-reversal state of the machine. The error bars indicate the 68% confidence level. The most important manual reversal is the electric-field reversal: the first four points correspond to one electric-field configuration, and the last four to the other. The solid and dashed lines show the mean value and its statistical error.

In addition to the computer-controlled switches, we make three manual reversals. The high-voltage connections are swapped to reverse **E**, the magnet wires are interchanged to reverse **B** and the r.f. cables are swapped to reverse the direction of r.f. propagation along the field plates. These manual changes are made infrequently—typically one switch per day—and they are valuable in identifying and eliminating systematic effects. Roughly equal numbers of blocks are taken in all eight of the manual states. When we divide the data according to these manual-reversal states and analyse each data set separately, the EDMs obtained are consistent with one another, as shown in Fig. 5. We also divide the data according to the polarization angles of the pump and probe and find no correlation with either.

Combining the systematic uncertainties in quadrature yields the final result $d_\mathrm{e} = (-2.4 \pm 5.7_\mathrm{stat} \pm 1.5_\mathrm{syst}) \times 10^{-28} e$ cm, where the first uncertainty is statistical (68% symmetric confidence interval[23]) and the second systematic. This is consistent with zero and with the previous best measurement[7]. The result is 54 times more precise than our previous measurement[8]. Treating the statistical and systematic errors on equal terms, we can extract an upper bound on the size of the EDM of $|d_\mathrm{e}| < 10.5 \times 10^{-28} e$ cm with 90% confidence. This is 1.5 times smaller than the previous upper limit[7].

Our error is dominated by the statistical uncertainty of the measurement. The limiting systematic errors in the measurement are sufficiently well understood that we can readily reduce them to the $10^{-29} e$ cm range. Our experiment leads the way in the application of cold molecule techniques to precision measurement and we are well placed to take advantage of recent advances in the preparation[24–26] and control[27] of cold molecules to improve our measurement precision. This will allow us to probe for new particle physics at tens of tera-electronvolts.

METHODS SUMMARY

Pulses of YbF are emitted by the source[17] every 40 ms and travel through the magnetically shielded apparatus (Fig. 1) at a speed of 590 m s^{-1}. The pump detector depletes and detects the $F = 1$ population while the probe detector measures the $F = 0$ population. Two r.f. π-pulses, separated by the free-evolution time T, and tuned to the Stark-shifted hyperfine interval near 170 MHz, coherently transfer molecules between the $F = 0$ and $F = 1$ states. The primary signal is the detected $F = 0$ population, which is proportional to $\cos^2\phi$. The electron EDM is obtained from the part of ϕ that correlates with the sign of E, which in turn is obtained from the signal correlating with the sign of $E \cdot B$.

To measure this correlation, and a rich set of other signal correlations, the machine is put into a new state between each beam pulse. There are nine switched parameters, and hence 512 different switch combinations; each is set eight times in every data block (a group of 4,096 pulses). For each block, the switching sequence is chosen at random from a set of possible sequences; all of these switch B frequently to eliminate magnetic field noise, switch E infrequently to minimize the dead time associated with this switch, and switch $E \cdot B$ aperiodically to eliminate signal drifts from this channel[28]. Between one block and the next, the relative phase of the two r.f. pulses is randomly changed, the linear polarizations of pump and probe are randomly rotated, and the central values of the magnetic field, the laser frequency, and the frequencies and amplitudes of the two r.f. pulses, are adjusted towards their ideal values.

Diagnostic data are obtained from a fluxgate magnetometer placed between the two shields, three other magnetometers around the laboratory, and two ammeters[22] that measure the currents flowing to the electric field plates.

Full Methods and any associated references are available in the online version of the paper at www.nature.com/nature.

Received 18 February; accepted 8 April 2011.

1. Khriplovich, I. B. & Lamoreaux, S. K. *CP Violation Without Strangeness* (Springer, New York, 1997).
2. Pospelov, M. & Ritz, A. Electric dipole moments as probes of new physics. *Ann. Phys.* **318,** 119–169 (2005).
3. Commins, E. D. Electric dipole moments of leptons. In *Advances in Atomic, Molecular, and Optical Physics* Vol. 40, 1–56 (eds Bederson, B. & Walther, H.), Academic Press (1999).
4. Commins, E. D. & DeMille, D. in *Lepton Dipole Moments* (eds Roberts, B. L. & Marciano, W. J.) Ch. 14 (World Scientific, Singapore, 2010).
5. Sakharov, A. D. Violation of CP invariance, C asymmetry, and baryon asymmetry of the Universe. *Pis'ma ZhETF* **5,** 32–35 (1967); *Sov. Phys. JETP Lett.* **5,** 24–27 (1967).
6. Edmonds, A. R. *Angular Momentum in Quantum Mechanics* 73–77 (Princeton University Press, 1996).
7. Regan, B. C., Commins, E. D., Schmidt, C. J. & DeMille, D. New limit on the electron electric dipole moment. *Phys. Rev. Lett.* **88,** 071805 (2002).
8. Hudson, J. J., Sauer, B. E., Tarbutt, M. R. & Hinds, E. A. Measurement of the electron electric dipole moment using YbF molecules. *Phys. Rev. Lett.* **89,** 023003 (2002).
9. Hinds, E. A. Testing time reversal symmetry using molecules. *Phys. Scr.* **T70,** 34–41 (1997).
10. Kozlov, M. G. & Ezhov, V. F. Enhancement of the electric dipole moment of the electron in the YbF molecule. *Phys. Rev. A* **49,** 4502–4507 (1994).
11. Kozlov, M. G. Enhancement of the electric dipole moment of the electron in the YbF molecule. *J. Phys. B* **30,** L607–L612 (1997).
12. Titov, A., Mosyagin, M. & Ezhov, V. P,T-odd spin-rotational Hamiltonian for YbF molecule. *Phys. Rev. Lett.* **77,** 5346–5349 (1996).
13. Quiney, H. M., Skaane, H. & Grant, I. P. *Hyperfine and PT-odd effects in YbF* $^2\Sigma$. *J. Phys. B* **31,** L85–L95 (1998).
14. Parpia, F. A. Ab initio calculation of the enhancement of the electric dipole moment of an electron in the YbF molecule. *J. Phys. B* **31,** 1409–1430 (1998).
15. Mosyagin, N., Kozlov, M. & Titov, A. Electric dipole moment of the electron in the YbF molecule. *J. Phys. B* **31,** L763–L767 (1998).
16. Hudson, J. J. *et al.* Pulsed beams as field probes for precision measurement. *Phys. Rev. A* **76,** 033410 (2007).
17. Tarbutt, M. R. *et al.* A jet beam source of cold YbF radicals. *J. Phys. B* **35,** 5013–5022 (2002).
18. Ma, T., Butler, C., Brown, J. M., Linton, C. & Steimle, T. C. Optical Zeeman spectroscopy of ytterbium monofluoride, YbF. *J. Phys. Chem. A* **113,** 8038–8044 (2009).
19. Maronna, R. A., Martin, D. R. & Yohai, V. J. *Robust Statistics; Theory and Methods* 31–32 (Wiley, 2006).
20. Efron, B. & Tibshirani, R. Bootstrap methods for standard errors, confidence intervals, and other measures of statistical accuracy. *Stat. Sci.* **1,** 54–75 (1986).
21. Tarbutt, M. R., Hudson, J. J., Sauer, B. E. & Hinds, E. A. Prospects for measuring the electric dipole moment of the electron using electrically trapped polar molecules. *Faraday Discuss.* **142,** 37–56 (2009).
22. Sauer, B. E., Kara, D. M., Hudson, J. J., Tarbutt, M. R. & Hinds, E. A. A robust floating nanoammeter. *Rev. Sci. Instrum.* **79,** 126102 (2008).
23. Efron, B. Better bootstrap confidence intervals. *J. Am. Stat. Assoc.* **82,** 171–185 (1987).
24. Skoff, S. M. *et al.* Diffusion, thermalization and optical pumping of YbF molecules in a cold buffer gas cell. *Phys. Rev. A* **83,** 023418 (2011).
25. Barry, J. F., Shuman, E. S. & DeMille, D. A bright, slow cryogenic molecular beam source for free radicals. Preprint at ⟨http://arxiv.org/abs/1101.4229⟩ (2011).
26. Hutzler, N. R. *et al.* A cryogenic beam of refractory, chemically reactive molecules with expansion cooling. Preprint at ⟨http://arxiv.org/abs/1101.4217⟩ (2011).
27. van de Meerakker, S. Y. T., Bethlem, H. L. & Meijer, G. in *Cold Molecules: Theory, Experiment, Applications* (eds Krems, R., Stwalley, W. & Friedrich B.) Ch. 14 (CRC Press, 2009).
28. Harrison, G. E., Player, M. A. & Sandars, P. G. H. A multichannel phase-sensitive detection method using orthogonal square waveforms. *J. Phys. E* **4,** 750–754 (1971).

Supplementary Information is linked to the online version of the paper at www.nature.com/nature.

Acknowledgements We acknowledge the contributions of P. Condylis and H. Ashworth. We are grateful for technical assistance from J. Dyne and V. Gerulis. This work was supported by the UK research councils STFC and EPSRC, and by the Royal Society. J.J.H. is supported by an STFC Advanced Fellowship.

Author Contributions J.J.H. was involved in all aspects of the measurement, led the analysis, and drafted the manuscript. D.M.K. developed many of the systematic tests, worked on taking the data set, and contributed to the analysis. I.J.S. had primary responsibility for taking the data set, and contributed to the development of the data acquisition techniques. B.E.S. was involved in all aspects of the measurement, and designed much of the hardware. M.R.T. built the molecular beam source, contributed to the analysis, and drafted the manuscript. E.A.H. contributed to the analysis, drafted the manuscript and led the team. All authors discussed the results, improved the manuscript and were equally involved in setting the direction of the work.

Author Information Reprints and permissions information is available at www.nature.com/reprints. The authors declare no competing financial interests. Readers are welcome to comment on the online version of this article at www.nature.com/nature. Correspondence and requests for materials should be addressed to E.A.H. (ed.hinds@imperial.ac.uk).

METHODS

Apparatus. The apparatus is shown in Fig. 1. A solenoid valve opens every 40 ms to release a pulse of Ar containing 2% SF_6. Ytterbium atoms laser-ablated from a target beside the valve react with the gas pulse to form YbF. The gas expands, cools and is skimmed to form a beam with a temperature of 3 K and a centre-of-mass velocity of 590 m s^{-1} (ref. 17). The YbF molecules are mainly in the electronic and vibrational ground state $X^2\Sigma^+(v=0)$. Those in the rotational ground state are distributed over the hyperfine levels $F=0$ and $F=1$, separated by 170.254 MHz. A single-mode continuous-wave dye laser provides the linearly polarized pump and probe beams shown in Fig. 1. The pump and probe are respectively tuned to the $F=1$ and $F=0$ components of the A–X $Q(0)$ transition, so that the pump empties out the $F=1$ population and the probe measures the $F=0$ population by laser-induced fluorescence detection. Each packet of molecules passing through the probe beam generates a current pulse in the photomultiplier corresponding to ~5,000 detected photons. The current pulse is digitized in 80 bins over 800 μs to produce signals such as that shown in Fig. 2. The pump fluorescence is recorded in a similar way. We also record the intensities of both laser beams. The timing of the experiment is phase-locked to the mains electrical supply.

The field plates are gold-coated cast aluminium, 75 cm long, 7 cm wide and 1.2 cm apart. The static electric and magnetic fields between these plates are typically $E=\pm 10$ kV cm^{-1} and $B=\pm 13$ nT. The plate structure doubles as a TEM (transverse electromagnetic) transmission line to propagate 170 MHz radiation in either direction. The r.f. pulses are designed to be π-pulses, so that the transfer of molecules between the $|F,m_F\rangle=|0,0\rangle$ state and the $\frac{1}{\sqrt{2}}(|1,+1\rangle+|1,-1\rangle)$ state occurs with unit efficiency. The first r.f. pulse is applied 1.1 ms after the ablation pulse, when the molecules are approximately 13 cm inside the plates. The second r.f. pulse is applied after the free evolution time of $T=642$ μs. Both pulses are 18-μs-long r.f. magnetic field pulses polarized along $\hat{\mathbf{x}}$ (Fig. 1). If the π-pulses are imperfect, coherence between $F=0$ and $F=1$ states results in additional, unwanted interference terms. We suppress these terms by averaging the relative r.f. phase $\phi_0 \pm \pi/2$ over the Φ_{rf} switch and by randomizing ϕ_0 between blocks. The theory of two-pulse r.f. transitions within this three-level manifold is developed fully in section IV.B of ref. 29.

The beam line is enclosed by two layers of magnetic shielding. The high-voltage feeds pass close together through a single hole in the inner magnetic shield near the centre of the plates to minimize shield magnetization by the charging currents. A fluxgate magnetometer between the shields measures the magnetic field parallel to $\hat{\mathbf{z}}$ near the probe detector. Three other magnetometers of lower sensitivity are used to monitor the laboratory magnetic field—one near the beam machine, one close to the high-voltage relays that reverse $\mathbf{E}$, and one close to the computer interface that controls the experiment. These are also read after every pulse and their primary purpose is to ensure that E-reversal does not generate a magnetic field. The same analogue–digital converter board that reads these signals also monitors two dummy voltages, a battery and a short circuit. These are used to check that there are no systematic errors in the signal processing electronics and data analysis.

Diagnostic data are also obtained from two ammeters[22] that measure the currents flowing to the electric field plates.

Characterizing the machine. We have mapped the spatial variation of the electric, magnetic and r.f. fields, as described in ref. 16. We find that the electric field varies by roughly 1% over the length of the plates, and that the ambient magnetic field is typically less than 10 nT throughout the region that we use for the interferometer. The r.f. field has a small standing-wave ratio, corresponding to a 4% power reflection coefficient at each end. In the TEM mode, the r.f. electric field is constrained by the same boundary conditions as the static field, ensuring that the r.f. magnetic field is accurately perpendicular to E and to the propagation direction. The r.f. field at each end of the plates has some ellipticity, due to the transient where the transmission line is coupled to coaxial cable. This decays away over a few centimetres.

Switching sequence. As discussed in the main text, nine separate parameters are switched in the experiment. A set of 4,096 beam pulses forms a block of data, within which all 512 combinations of switch states are covered equally. The sequence of switches applied within a block, known as the switching pattern, must satisfy three requirements. First, the magnetic field should switch frequently to eliminate magnetic field noise. Second, the electric field must switch less often because E reversal incurs a dead time of 14 s. This allows time to discharge and recharge the plates while keeping the transient currents below 5 μA to avoid magnetizing the shields. By the time we restart data acquisition the current is close to its steady value of ~1 nA. This restriction is important because a magnetic field reversing with E can generate a systematic error. Third, the switching sequence of $E \cdot B$ should be as aperiodic as possible so that signal drifts do not influence this channel[28]. Within these restrictions, there are still a large number of possible switching patterns from which the computer randomly chooses one at the start of every block. At the end of each block the channel values are calculated and some of these are used to optimize the running of the machine. For example, $\{B\}$ measures how well the operating fields are centred around $B=0$ and this provides an error signal at the end of each block that is fed back to compensate for small drifts of the ambient field. Similarly, $\{v_{rf1}\}$ and $\{v_{rf2}\}$ are used to lock the r.f. frequencies to resonance while $\{a_{rf1}\}$ and $\{a_{rf2}\}$ are used to lock the r.f. amplitudes to the π-pulse condition. The laser- frequency channel {LF} is used to keep the laser on resonance. Between blocks the mean relative phase ϕ_0 between the two r.f. pulses is randomly changed and the linear polarizations of the pump and probe laser beams are randomly rotated. Including the dead time, each block takes approximately 6 min to accumulate.

EDM interaction. The interaction of the electron in a molecule with an applied electric field is more complicated than that of a free electron, described in the introduction. It is possible however to write the interaction as $-\mathbf{d}\cdot\mathbf{E}_{eff}$. The effective electric field $\mathbf{E}_{eff}$, which depends nonlinearly on the applied electric field, accounts for the complexity of the molecular environment. Under our operating conditions the effective field has magnitude 14.5 GV cm^{-1} and is aligned antiparallel to the applied field[10–15]. Thus, the energy shift of the $(F=1,m_F)$ state of the molecule due to the electron EDM is $-d_e E_{eff} m_F$ where $E_{eff}=-14.5$ GV cm^{-1}. In deriving the EDM we have assumed that the effective field is known exactly. Although there is some uncertainty in the theoretical calculation, even an uncertainty of 10% would have no impact on our error at the level reported here.

29. Tarbutt, M. R., Hudson, J. J., Sauer, B. E. & Hinds, E. A. in *Cold Molecules: Theory, Experiment, Applications* (eds Krems, R., Stwalley, W. & Friedrich B.) Ch. 15 (CRC Press, 2009).